STUDIA UBB CHEMIA, LXX, 3, 2025 (p. 265-279)
(RECOMMENDED CITATION)
DOI:10.24193/subbchem.2025.3.18

SPECTROSCOPIC AND THERMAL ANALYSES OF THE INHIBITORY MECHANISM OF *OKANIN* ON *XANTHINE OXIDASE*

Meng-Rong LI[a], Mu-Xin LIU[a,*], Wei LIU[a], Rui HE[a], Shan-Bin JIANG[a], Shen-Qiang LI[a]

ABSTRACT. Okanin was identified as a xanthine oxidase inhibitor, and for the first time, the thermodynamic parameters of the interaction—including entropy change (ΔS), enthalpy change (ΔH), and Gibbs free energy (ΔG)—were calculated by combining fluorescence spectrometry and differential thermal scanning. It can be inferred that there exists a hydrogen bond between okanin and XO, with the van der Waals force being the predominant intermolecular force between them. Nuclear Magnetic Resonance Hydrogen Spectroscopy (^{1}H-NMR) not only confirmed the presence of hydrogen bonding but also provided initial predictions of the specific binding location of the inhibitor and enzyme. Three-dimensional and synchronous fluorescence demonstrated that okanin induces structural modifications in the enzyme, leading to inhibition. Molecular docking directly revealed the binding pattern between inhibitor and enzyme, which aligned with the aforementioned experiments. The findings indicated that inhibitors were competitively bound to the enzyme's active site primarily through intermolecular forces such as hydrogen bonding, conjugation, and van der Waals forces. These interactions facilitate the formation of a stable intermediate, inducing structural changes in the enzyme, and enhancing the inhibitory ability of okanin. Antioxidant experiments showed that okanin further inhibits the generation of O_2^- free radicals by simultaneously promoting the reduction of XO molecules and suppressing the production of uric acid. Hence, okanin shows promise as a novel natural product that inhibits the activity of xanthine oxidase, making it highly significant to investigate its potential anti-gout properties.

Keywords: *Okanin; differential thermal scanning; Nuclear magnetic.*

[a] *Bengbu University, School of Materials and Chemical Engineering, Longzi Lake District, 233030, Bengbu, China.*
[*] *Corresponding author: limr@bbc.edu.cn*

INTRODUCTION

Elevated levels of uric acid in the bloodstream are widely recognized as a leading cause of hyperuricemia. Progressive hyperuricemia leads to the deposition of monosodium urate crystals, which can trigger gout pathogenesis. The presence of these crystals within the joints can stimulate the synovial membrane, resulting in joint swelling, deformity, and pain for affected individuals. In severe cases, this can also impede joint mobility. Si et al. [1] discovered a positive correlation between uric acid levels and the incidence of type 2 diabetes in many patients. The body normally maintains stable uric acid levels, but an imbalance in uric acid metabolism can lead to hyperuricemia. Current pharmacological interventions, including xanthine oxidase inhibitors and uricosuric agents, while effective in reducing uric acid production and enhancing excretion, are frequently associated with adverse effects [2]. Therefore, it is crucial to investigate the effects and mechanisms of natural plant-derived active ingredients with pharmacological properties on uric acid synthesis and the activity of related enzymes in order to develop new and safe drugs for lowering uric acid levels.

Xanthine oxidase (XO), is present in various organisms and is commonly found in the liver and kidney of mammals, bacteria, insects, and birds. It facilitates the conversion of purine to uric acid [3]. The crystal structure of xanthine oxidase consists of 1330 amino acids with a 90% similarity in sequence between mice and humans. It is composed of two symmetrical structural units known as homologous dimers, each weighing 145 kDa. The catalytic center includes one molybdenopterin center, two iron-sulfur centers, and one flavin adenine dinucleotide. Among these components, the molybdenopterin center plays a key role in catalyzing the production of uric acid from xanthine [4].

Natural products have emerged as a significant research focus for some scholars due to their attributes of safety, non-toxicity, abundant availability, and strong biological activity. They play a crucial role in the food and biomedicine industries, providing essential guidance for current research on plant active ingredients. Okanin, a principal bioactive flavonoid constituent of Coreopsis tinctoria (Asteraceae family), represents a promising candidate for therapeutic development [5]. Studies have demonstrated its anti-inflammatory, antioxidant, and vascular growth promotion effects in mice [6]. Shi et al investigated okanin's inhibitory effect on two metabolic subtypes of CYP3A4 and CYP2D6 enzymes, suggesting its potential use as a diabetes treatment drug [7]. However, the interaction mechanism between okanin and XO remains unclear; therefore, this experiment selected okanin as an inhibitor to study its inhibition mechanism on XO.

Various methods were employed for the first time to investigate the inhibitory activity and interaction of okanin on XO. The binding constant and interaction force between inhibitor and enzyme were quantitatively analyzed using various spectral methods and differential thermal scanning, which also revealed conformational changes in enzyme structure. ^{1}H NMR could infer hydrogen bond formation and binding sites through variations in hydrogen displacement, while molecular docking provided a direct visualization of the binding diagram between inhibitor and enzyme. This study is valuable for investigating the intermolecular interactions between the okanin and xanthine oxidase, offering a promising approach to exploring the mechanism of inhibitor inhibition on the enzyme, ultimately leading to the discovery of a novel and efficient XO inhibitor.

RESULTS AND DISCUSSION

Experiment of okanin inhibiting enzyme activity.The experimental data of inhibition of enzyme activity demonstrated that okanin exhibited a stronger xanthine oxidase (XO) inhibitory activity than allopurinol, as indicated by its lower IC_{50} value (2.30 μM) in comparison to allopurinol (7.36 μM). This suggests the potential for further exploration of okanin as a new inhibitor. The enhancement of inhibition may be due to the hydroxyl group contained in the benzene ring structure being bonded to the XO active cavity by hydrogen bonding. This interaction appears to movement of hydrogen atoms in the propylene group towards the benzene ring and reduction in electron cloud density of the carbon atoms within the propylene group, thereby achieving highly efficient enzyme inhibition. It was also possible that the enzyme activity was reduced by inhibiting the O_2^- free radicals, the product of xanthine catalyzed by XO.

Inhibition mechanism, inhibition principle. The inhibitory mechanism of okanin on xanthine oxidase was evidented from the Figure 1(A), which shows a linear plot passing through the origin of coordinates. The slope of the curve is inversely proportional to the concentration of the inhibitor. The concentration-dependent decrease in slope confirmed okanin as a reversible inhibitor of XO [8]. The type and inhibition constant of okanin on XO could be determined using the Lineweaver–Burk plot as depicted in Figure 1(B), where four lines intersect at the Y-axis. This indicates that okanin competes with xanthine for binding in the active cavity of XO. Therefore, it is a competitive XO inhibitor [9]. Furthermore, based on the relationship between slope and concentration in Figure 1(C), a K_{IS} value of 0.16 μM suggests that okanin competitively binding to allopurinol at the active center of enzyme, significantly reducing enzymatic activity.

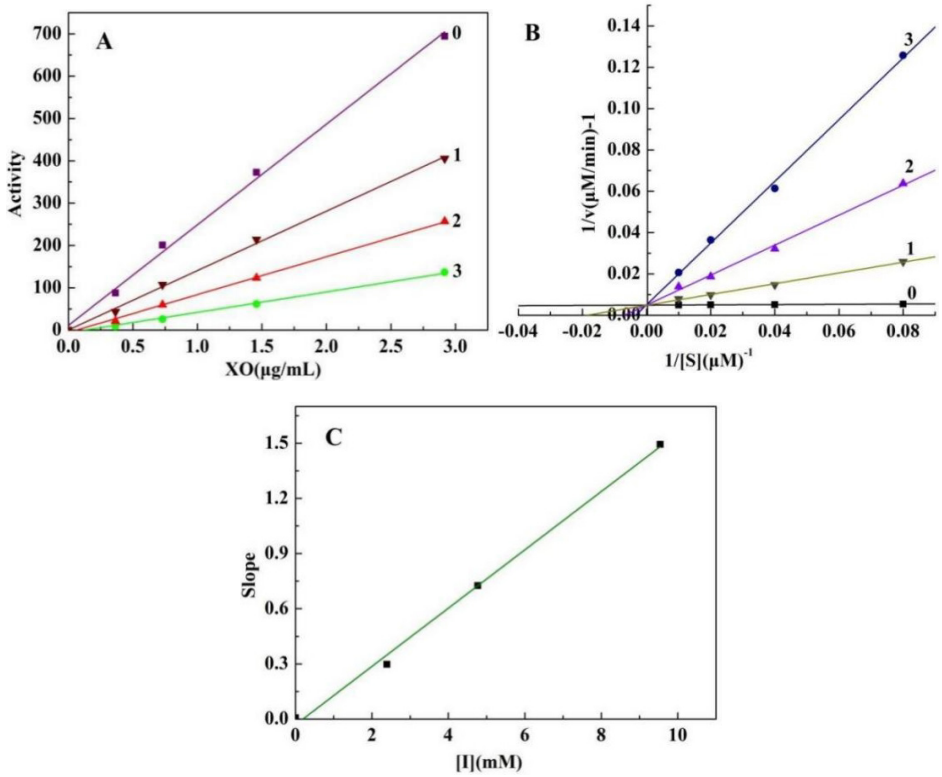

Figure 1. The inhibitory effects of okanin on XO (A). The concentration of curve 0-3 for okanin were 0, 2.39, 4.77, 9.54 mM, respectively; Lineweaver–Burk plots of okanin on XO (B). The concentration of xanthine were 0.02, 0.04, 0.08, 0.15 mM, respectively. The plot of the slope for okanin (C).

Fluorescence quenching. The technique of fluorescence quenching had been commonly utilized to investigate ligand-protein interactions. The fluorescence emission spectra of each solution were depicted in Figure 2(A). It was evident that the fluorescence intensity of XO in aqueous solution at 400 nm was significantly higher than at other wavelengths. Progressive addition of okanin resulted in concentration-dependent quenching of XO fluorescence, which proved that okanin could quench the fluorescence intensity of XO. Stern-Volmer curves at different temperatures revealed two quenching patterns: static quenching and dynamic quenching. As can be seen from the Figure 2(B), The Stern-Volmer curve was divided into two linear intervals, suggesting both dynamic and static modes of fluorescence quenching between okanin and XO. As compound concentration increased, the Stern-Volmer curve approached

the Y-axis, indicating a shift towards more dynamic quenching for XO compounds with higher concentrations. By using a compound concentration of 32.10 μM as the cut-off point, the corresponding Ksv was determined through piecewise linear fitting of Stern-Volmer curves. The Table 1 results presented in the table indicate that the apparent quenching constant significantly exceeds the maximum diffusion impact quenching constant (2.0×10^{10} $L.mol^{-1}.S^{-1}$) [10]. The above results are summarized that the interaction between the compound and enzymes is primarily attributed to static quenching. However, with increasing compound concentration, the influence of dynamic quenching became more prominent. It is evident from the table that both okanin and XO exhibit similar apparent binding sites and binding constants, with an apparent binding constant below 0.08 mol/L indicating non-covalent complex formation through interactions such as hydrophobic interaction and hydrogen bonding [11].

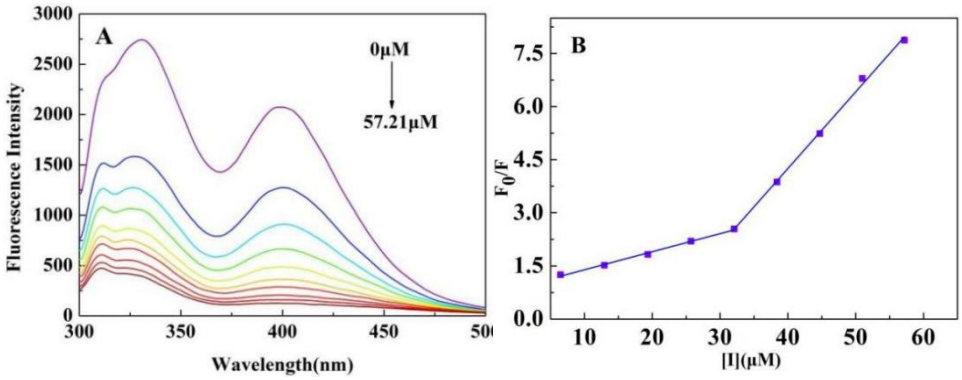

Figure 2. Fluorescence mapping of the interaction between okanin and XO (A) and the Stern–Volmer plot (B). Concentrations for curves were 0-57.21 μM, respectively. The temperature was 303 K.

Table 1. Apparent extinction constants of 303 K interactions between okanin and XO.

Complex	C(μmol·L^{-1})	K_{SV}(10^4L·mol^{-1})	Kq(10^{12}L·mol^{-1}·S^{-1})
Okanin-XO	≤32.1	0.05	0.05
	>32.1	0.22	0.22

The binding constant (Ka) of the inhibitor to the enzyme is obtained by the following formula [12]:

$$\lg\frac{F_0 - F}{F} = \lg K_a + n\lg[Q]$$

Analyzing the data in table 2, When the temperature changed from 298 K to 303 K, there was a significant increase in the Ka value, indicating that the binding affinity of the inhibitor to the enzyme and the formation of hydrogen bonds are closely related to the hydrophobic effect. Subsequently, temperature further increased from 303 K to 308 K, the disruption of hydrogen bonds led to a significant decrease in Ka value, indicating that okanin and enzyme predominantly bond through hydrogen bonding.

Analysis of differential scanning calorimeter test results. Differential scanning calorimeter (DSC), as an experimental tool of differential scanning calorimetry, is widely used in thermal analysis. In this experiment, a dynamic model was employed where the temperature of the sample pool and the reference pool increased simultaneously at a set heating rate to analyze the thermal behavior of the sample under external heating conditions. The system exhibited a progressive decrease in heat flow from 298 K to 308 K, resulting in a gradual decline in the DSC curve. Within this temperature range, software automatically calculates ΔH to be -3.821 J/g, indicating an energy change between okanin and XO leading to complex formation.

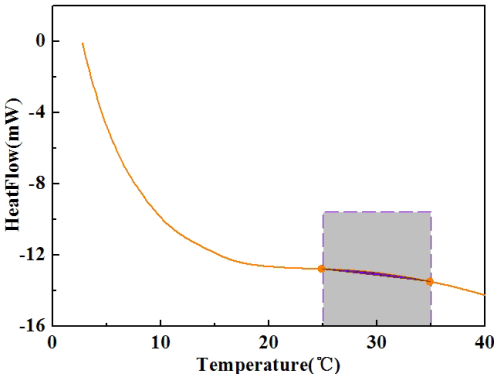

Figure 3. DSC curve of heat flow rate with temperature in okanin and XO mixed system.

Measurement of thermodynamic parameters. On the basis of fluorescence and differential thermal scanning experiments, the Thermodynamically related data during the formation of the complex were calculated according to the formula [13], and the interaction force between okanin and XO was judged successively.

$$\lg K_a = -\frac{\Delta H}{2.303RT} + \frac{\Delta S}{2.303R}$$
$$\Delta G = \Delta H - T\Delta S$$

Table 2. Bind constants and thermodynamic parameters for the interaction of XO with okanin at different temperatures.

Complex	Temperature (K)	K*a* (10^4L.mol^{-1})	ΔH (KJ.mol^{-1})	ΔG (KJ.mol^{-1})	ΔS (KJ.mol^{-1})
Okanin-XO	298	1.09	-13.28	11.19	-37.58
	303	5.15		11.40	
	308	0.44		11.59	

Analysis of the thermodynamic parameters in Table 2 revealed negative values for ΔG, ΔH, and ΔS. A negative Gibbs free energy change (ΔG < 0) indicated that acarbose spontaneously binds to XO. A negative enthalpy (ΔH < 0) and entropy change (ΔS < 0) indicated that van der Waals forces and hydrogen bonds were the main forces for acarbose binding to the enzyme. These thermodynamic findings, combined with the results of fluorescence quenching experiments, concluded that okanin forms a stable complex with the enzyme through these two forces.

Synchronous fluorescence experiment. XO contains fluorescein groups tyrosine and tryptophan residues, and their fluorescence peaks could reflect the conformational changes of XO. Spectral analysis revealed a 2 nm red shift (Δλ=15 nm) in the Tyr emission maximum. This phenomenon indicated a change in the enzyme microenvironment, with implications for enhanced hydrogen bonding force around hydrophilic amino acid residues such as tyrosine. These findings further corroborated the presence of hydrogen bonding forces in the interaction between okanin and XO. The synchronous fluorescence quenching rate (RSFQ) could be determined by substituting the experimental synchronous fluorescence data into the following formula [14]: $\mathrm{RSFQ} = 1 - \mathrm{F}/\mathrm{F}_0$, where F represents the fluorescence intensity of XO and F_0 represents the fluorescence intensity of inhibitor and enzyme binding [15]. As shown in figure 4(C), it was evidented that at the same concentration of okanin, the RFSQ values for tryptophan (∆λ=60 nm) were notably higher than those for tyrosine (∆λ=15 nm). This observation suggests that tryptophan residues may have a greater impact on the fluorescence quenching of XO compared to tyrosine residues, possibly due to their closer proximity to okanin.

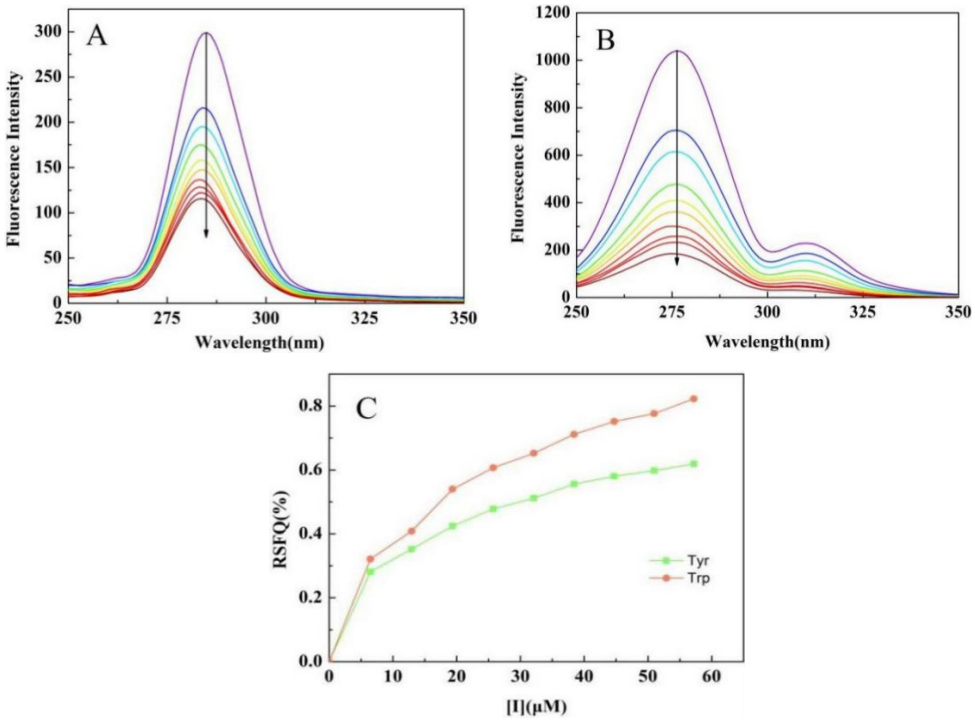

Figure 4. The synchronous fluorescence spectra. Δλ=15 nm (A) and Δλ=60 nm (B), and RSFQ values of Tryptophan and tyrosine residues are present in XO structures (C). Concentrations for curves were 0-57.21 μM, respectively.

Three-dimensional fluorescence. Three-dimensional fluorescence spectroscopy was utilized for investigating alterations in protein structure and microenvironment [16]. Figure 5 displayed four distinct fluorescence emission peaks, including the Rayleigh scattering peak (peak 1), tyrosine residue fluorescence emission peak (peak 2), tryptophan residue fluorescence emission peak (peak 3), skeleton structure of XO (peak 4) [17]. Each peak was represented by a different color-filled region in the figure, with colors deepening from the outside to the inside and corresponding to an increase in fluorescence intensity. Compared to the blank XO (Figure 5A), the enclosed region of each peak in the three-dimensional fluorescence (Figure 5B) resulting from the addition of a certain concentration of okanin was reduced, with a noticeably lighter color indicating decreased fluorescence intensity. The identical conclusion was reached through fluorescence titration experiment. However, there was a stronger impact on the change of tryptophan residues at peak 3 compared to tyrosine residues at peak 2, This certificated that tryptophan residues more

significant impact than tyrosine residues in the binding of the inhibitor to XO. This phenomenon may be attributed to the formation of a complex between okanin and XO, which alters the spatial conformation of XO.

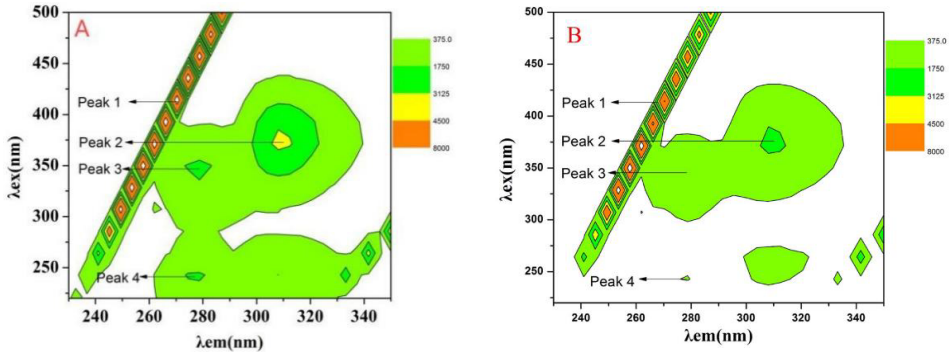

Figure 5. Three-dimensional fluorogram of XO (A) and okanin added in XO (B)

Nuclear Magnetic Titration. Nuclear magnetic titration was a method used to predict the binding site of small molecules on large molecules by analyzing the change in chemical shift of hydrogen atoms within small molecules when they interact with large molecules [18]. As shown in Figure 6, the hydrogen atoms (13.59, 10.09, 9.75, 9.10, 8.60 ppm) on all hydroxyl groups of okanin structure disappear immediately while the CH protons suffer no change in position or in intensity after the addition of a small amount of enzyme solution.

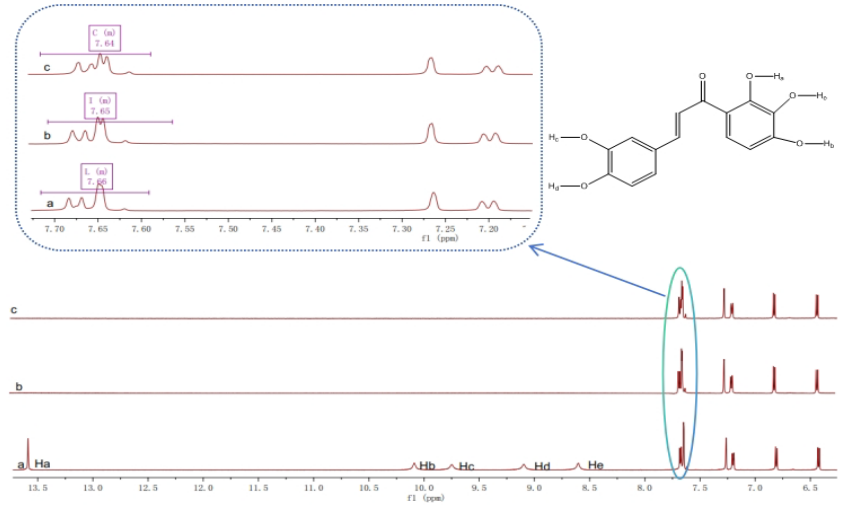

Figure 6. ^{1}H NMR titration of okanin with XO in DMSO-d_6.
Concentrations of XO for curves a-c were 0, 0.2, 0.4 mg/μL.

This could be explanation may be that the OH protons of okanin have been exchanged with deuterium. Figure 6 also indicated that due to the peak splitting of olefin groups, the electron could density increases. This could be attributed to the oxygen atoms within the carbonyl group in okanin's structure forming hydrogen bonds with the enzyme, induced electron cloud density enhancement, thereby enhancing the inhibitory ability of okanin.

Molecular docking. To comprehend the precise binding site and interaction force of inhibitor with XO, molecular docking of okanin was conducted using Accelrys Discovery Studio 4.2 software [19]. Figure 7 clearly illustrated okanin occupies the catalytic center of XO with a potential energy of -28.49 kcal/mol. Purple representing the donor and green representing the receptor. The cavity was identified as a hydrogen bond cavity, indicating the presence of hydrogen bonds. Additionally, a 2D diagram in Figure 7(B) demonstrated that okanin forms hydrogen bonds with amino acid residues such as THR1083, SER1080, LYS1045, GLY1039, GLY797, PHE798 to facilitate its combination with XO. Furthermore, okanin may enhance cavity stability by forming van der Waals forces with ALA1258, ASP1084, VAL1081, SER1082, ALA1078, GLY799, GLY796, GLN1194, GLY1260, and VAL1259. The enzyme-inhibitor primary intermolecular forces was hydrogen bonds and van der Waals forces, which aligned with experimental results from fluorescence and nuclear magnetic titration studies.

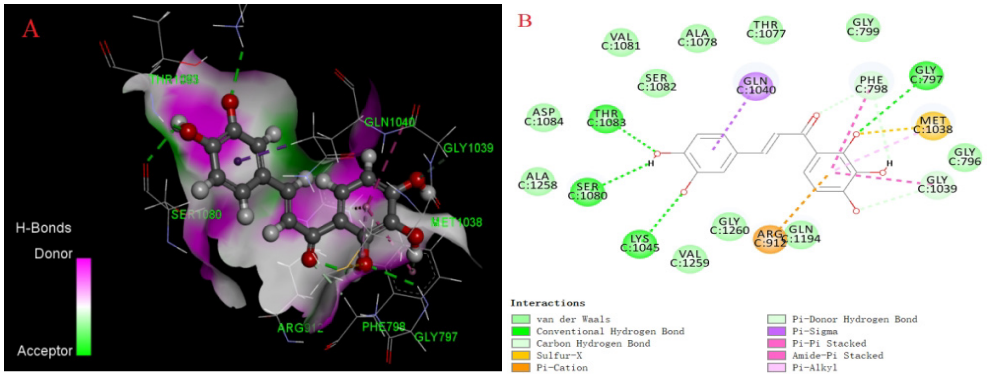

Figure 7. Molecular docking diagram(A) and 2D structure diagram(B).

Antioxidant experiment. The antioxidant experiment could obtain the inhibitory ability of okanin on the generation of O_2- free radicals by XO catalysis. Figure 8 showed the antioxidant activity of okanin in the XO reaction system. It could be seen from Figure 8(A) that the experimental system had obviou absorption at 560 nm. The absorbance of XO decreased significantly after

gradually adding okanin, indicating that okanin could inhibit the O_2- free radical in the product of the XO reaction system. Figure 8(B) proved that O_2- radicals could be inhibited when the concentration of the inhibitor was within the range of 0.81μM, and subsequently the change in inhibitory activity was not obvious. The above results indicated that the reduction of O_2- radicals catalyzed by XO was due to the inhibitory effect of okanin. The IC_{50} value of okanin in inhibiting the generation of O_2- free radicals is 2.25μM, which was similar to the IC_{50} value for inhibiting the production of uric acid. It indicated that okanin further inhibited the generation of O_2- free radicals by simultaneously promoting the reduction of XO molecules and inhibiting the production of uric acid [20].

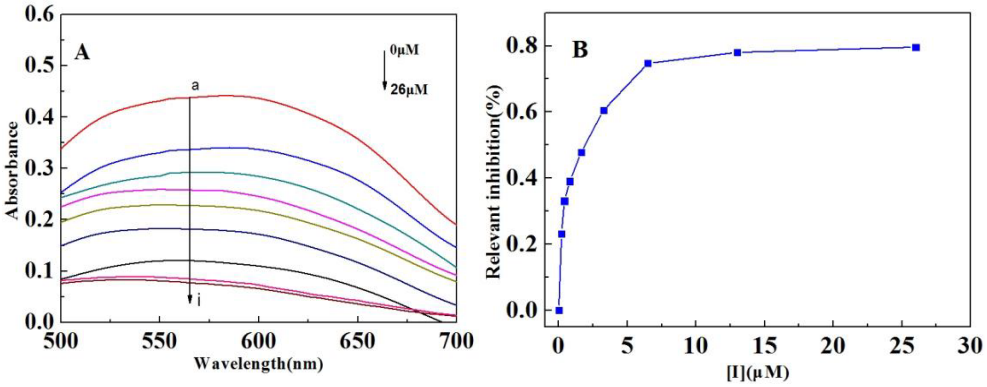

Figure 8. UV spectrum of the reaction between okanin and the O_2- radical catalyzed by XO (A); The inhibition rate of okanin on the O_2- radical of the XO catalytic product (B).

CONCLUSIONS

This study utilized UV spectroscopy, fluorescence spectroscopy, differential thermal scanning, ^{1}H NMR, and molecular docking to systematically investigate okanin's inhibition mechanism against xanthine oxidase. The results showed that okanin competitively bound in the active center of enzyme as indicated and proved that okanin could inhibit the production of O_2- radicals by promoting the reduction of XO molecules by ultraviolet spectroscopy. Fluorescence spectroscopy confirmed that static quenching dominance. Differential thermal scanning provided enthalpy change data for okanin and enzyme binding within the experimental temperature range. More precise thermodynamic parameters obtained through combination with fluorescence spectra. The findings indicated that hydrogen bonding and van der Waals

forces played crucial roles in facilitating the interaction between inhibitor and enzyme, leading to the inhibition of enzyme activity. ^{1}H NMR and molecular docking technology could support this conclusion. In summary, okanin and xanthine competitively bind in the core of XO, forming stable intermediates through hydrogen bonding, van der Waals force, conjugation, and other forces, inducing structural changes of the XO. As a potential new xanthine oxidase inhibitor, okanin presents a promising avenue for further research into gout and hyperuricemia treatment strategies.

EXPERIMENTAL SECTION

Reagents and Materials. Xanthine oxidase (EC 1.2.3.2, from bovine milk, US, Sigma), Xanthine (US, Sigma), Dimethyl sulfoxide (Tianjin, Damao Chemical Reagent), $NaH_2PO_4.2H_2O$ (Nanchang, Xilong Chemical), $Na_2HPO_4.12H_2O$ (Nanchang, Xilong Chemical), Okanin (Chengdu, Reifensi Biotechnology), Ethanol absolute (Tianjin, Damao Chemical Reagent Factory). The reagents used in the experiment were all analytically pure.

Enzyme activity. The experiment method was modified on the basis of previousreference slightly [21]. This activity assay system was incubated one minute at 30℃, contains 0.85 mL 0.05 M PBS buffer (Na_2HPO_4-NaH_2PO_4, pH=7.5), 2 mL 0.15 mM xanthine, 0.05 mL okanin solution and 0.1 mL XO. Among them, xanthine was substrate. The absorbance value of the product was measured at 285 nm, The enzyme activity value could be read directly through the software interface, and inhibit 50% of the enzyme activity (IC_{50}) was calculated by IBM SPSS Statistics software. The formula for calculating the inhibition rate is:

$$\text{Inhibition rate } (\%) = \frac{OD_2 - OD_1}{OD_2} \times 100\%$$

Where OD_1 and OD_2 are the enzyme activity values of the activity assay system in the presence and absence of inhibitors.

Dynamic mechanism experiment. The concentration of XO was varied while keeping the substrate concentration fixed in this assay. Different concentrations of okanin solution were mixed into systems, which containing different concentrations of enzymes and substrates. A series of correlation curves between enzyme concentration and activity value were then generated to judge the inhibitory principle of the inhibitor-XO. The opposite approach to the inhibition mechanism involved maintaining a constant XO concentration while varying the substrate concentration. The inhibition type can be characterized using the Lineweaver-Burk equation [14]:

$$\frac{1}{v} = \frac{K_m}{V_m}\left(1 + \frac{[I]}{K_I}\right) + \frac{I}{V_m}\left(1 + \frac{[I]}{K_{IS}}\right)$$

V represents velocity and K represents a constant. V_m denotes the maximum reaction rate;K_I is the binding constant of okanin with the free enzyme; K_{IS} is the binding constant of okanin with the complex in the solution system, and K_m is Michaelis constant; [*I*] is the inhibitor concentration.

Fluorescence quenching assay. The experimental method was conducted by making slight modifications to a previous article [22]. In the experimental setup, a base solution consisting of 1.8 mL phosphate buffer and 0.2 mL XO solution was utilized. Okanin solution was then titrated into the system using a micropipette, with the final concentration reaching 57.21 μM. The fluorescence intensity of the inhibitor was measured at an excitation wavelength of 278 nm and emission wavelength of 300-500 nm. Three different temperatures (298 K, 303 K, and 308 K) were selected for the experiment. To correct for UV absorption at this wavelength, the following formula was utilized [23]:

$$F_{corr} = F_{obs} e^{(A_1 + A_2)/2}$$

F_{corr} represents the precise fluorescence intensity value, while F_{obs} denotes the fluorescence intensity value measured. A_1 and A_2 stand for the absorbance values at the excitation and emission wavelengths respectively.

The Stern-Volmer equation is as follows [24]:

$$\frac{F_0}{F} = 1 + K_q \tau_0 [Q] = 1 + K_{SV}[Q]$$

F represents the fluorescence intensity of the enzyme; F_0 denotes the fluorescence intensity of the system upon addition of the inhibitor. K signifies the constant; where K_q stands for the rate constant, K_{SV} is the quenching constant; τ_0 indicates the average fluorescence lifetime of the enzyme, and [*Q*] denotes the concentration of the inhibitor.

Experimental study of differential scanning calorimetry. The DSC131 Evo differential scanning calorimeter produced by SETARAM, France, was used in this experiment. High purity nitrogen was used as a purge gas. And a drying gas with a purge rate was 30 mL·min^{-1} while a drying gas rate of 100 mL·min^{-1}. The heating rate is 5K·min^{-1}, these instrument should be calibrated before the experiment. The reference pool and the sample pool were placed in the instrument at the same time. The mixed solution of okanin and XO was placed in the sample pool, and the experimental temperature was set to 0-40℃.

Three-dimensional fluorescence. The reaction system was composed of 1.8 mL of PBS buffer solution, 0.2 mL of xanthine oxidase solution, and 5 μl of 1 mM inhibitor added step by step. The excitation and emission wavelengths must be configured. For this experiment, the excitation wavelength is set to begin at 200 nm, while the emission wavelength range is 200-350 nm, and using a slit width of 5 nm.

Synchronous fluorescence. The solution was prepared following the same procedure as for the three-dimensional fluorescence experiment. Excitation and emission wavelengths were set within the ranges of 200-350 nm and 200-500 nm, with intervals of 15 and 60, respectively. The slit widths were set at 5nm to scan the synchronous fluorescence spectrum.

Nuclear Magnetic Titration. A solution of 2.5 $mg \cdot mL^{-1}$ okanin in DMSO-d_6 was prepared and titrated with a 0.2 $mg \cdot \mu L^{-1}$ xanthine oxidase solution using a micropipette. The 1H NMR spectrum was recorded after each addition of xanthine oxidase, and the perturbation of hydrogen atoms in the spectra was assessed for comparison.

Molecular simulation experiment. In this study, Accelrys Discovery Studio 4.2 software was used to interface okanin with the Mo-pt active center of XO. The X-ray crystal structure of XO (PDB ID: 1FIQ) is available from the RCSB protein database (http://www.rcsb.org/pdb). All water and excess ligands need to be removed from the crystal structure before docking. The docking procedure based on CHARMm was used to dock the small molecule conformation in the receptor active site region, and finally optimize it to obtain the most accurate docking results. The docking structure with the highest score was selected to analyze its combination mode.

Antioxidant experiment. The mixed solution of NBT and xanthine (1:5), 2mg/μL XO solution and different concentrations of okanin (0-26 μM) solution were incubated in a 37 ° C water bath for half an hour. 1mL of standby mixture, 0.1mL XO solution and 0.75mL PBS ((Na_2HPO_4-NaH_2PO_4, pH=7.5)) buffer solution were added to the cuvette. Then, introduced different concentrations of okanin solution and measured the wavelengths-dependent absorbance changes of the system at range of 500 to 700 nm.

ACKNOWLEDGMENTS

This work was supported by the Anhui Provincial universities natural science research key project (KJ2021A1123), Anhui Province excellent young teacher training project (YQZD2023082), Quality Engineering Project of Anhui Province “Material Science and Engineering Teaching Innovation Team” (2023cxtd106) and Bengbu University Natural Science Research Project (2023ZR01). Their support was instrumental in the completion of this research.

REFERENCES

1. N van der Schaft; A Brahimaj; K Wen; OH Franco; A Dehghan; *PloS one*, **2017**, 12, e0179482.
2. S Gong; J Song; L Wang; S Zhang; Y Wang; *Eur J Gastroen Hepat,* **2016**, 28, 132-138.
3. J Gao; X Liu; B Zhang; Q Mao; Z Zhang; Q Zou; X Dai; S Wang; *Eur J Med Chem*, **2020**, 190, 112077.
4. R Rullo; C Cerchia; R Nasso; V Romanelli; ED Vendittis; M Masullo; A Lavecchia; *Antioxidants*, **2023**, 12, 825.
5. Q Yang; Y Sun; L Zhang; L Xu; M Hu; X Liu; F Shi; *J Herb Med*, **2014**, 6, 103-109.
6. Y Mi; J Xu; R Shi; Q Meng; L Xu; Y Liu; T Guo; D Zhou; J Liu; W Li; N Li; Y Hou; *Food Funct*, **2023**, 14, 369-387.
7. Y Shi; J Xie; R Chen; G Liu; Y Tao; Y Fan; X Wang; L Li; J Xu; *Biomed Chromatogr*, **2021**, 35, e5039.
8. C.M. Hu; Y.Y. Zheng; A.T. Lin; X Zhang; X.Z. Wu; J Ling; X.T. Xu; Z Xiong; *J Mol Struct*, **2023**, 1271, 134124.
9. Y Wang; G Zhang; J Pan; D Gong; *J Agr Food Chem*, **2015**, 63, 526-534.
10. L Liu; M Yuan; S Huang; J Li; D Li; L Zhao; *Appl Sci*, **2018**, 8, 158.
11. B Pan; B Xing; W Liu; G Xing; S Tao; *Chemosphere*, **2007**, 69, 1555-1562.
12. X.K. Su; Z.C. Sun; C.Y. Zhao; H Yang; T.M. Zhao; C Ma; G.F. Zhu; *J Spectrosc*, **2024**, 9923310.
13. K Rajeshwari; P Vasantha; B Shekhar; PV Anantha Lakshmi; *Appl Biochem Biotech*, **2022**, 194, 2650-2671.
14. M Li; Y Yu; J Liu; Z Chen; S Cao; *J Mol Struct*, **2018**, 1159, 23-32.
15. N Zeng; G Zhang; X Hu; J Pan; Z Zhou; D Gong; *J Funct Foods*, **2018**, 50, 172-182.
16. Y Gao; Z Wang; Y Li; H Luo; Z Zhou; *Spectrochim Acta A*, **2021**, 248, 119230.
17. L Chen; M Zhu; X Hu; J Pan; G Zhang; *J Sci Food Agr*, **2022**, 102, 3835-3846.
18. J Xu; J Liu; X Zhu; Y Yu; S Cao; *Food Chem*, **2017**, 221, 1530-1538.
19. R.K. Chaudhary; S.S. Karoli; P.S.R. Dwivedi; R Bhandari; *J Diabetes Metab Dis*, **2022**, 21, 445-454.
20. N Masuoka; I Kubo; *BBA-MOL BASIS DIS*, **2004**, 1688, 245-249.
21. N Zeng; G Zhang; X Hu; J Pan; D Gong; *J Funct Foods*, **2019**, 58, 1-10.
22. C Koffler; K Rohde-Brandenburger; *Int J Life Cycle Ass*, **2019**, 24, 397-399.
23. S Bi; Y Sun; C Qiao; H Zhang; C Liu; *J Lumin*, **2009**, 129, 541-547.
24. J Xie; H Cui; Y Xu; L Xie; W Chen; *FQS*, **2021**, 5, fyaa038.